Activity based Deubiquitinase profiling reveals OTUB1 from oryza sativa Hydrolyzes Linear Ubiquitin Chains by Bi-modal Activation

Lining Lu (thu20151@sina.com)
Guangxi University
Jiawei Wang
Tsinghua University
Ziqing Mei
University of Science and Technology Beijing
Feng Wang
Beijing Institute of Technology

Article

Keywords: Deubiquitination, Inflammation, Innate Immunity, Distal and Proximal Ubiquitin, Hydrolytic Ability, Metazoans

Posted Date: February 15th, 2021

DOI: https://doi.org/10.21203/rs.3.rs-199392/v1

Version of Record: A version of this preprint was published at Nature Communications on August 9th, 2022. See the published version at https://doi.org/10.1038/s41467-022-32364-3.

Abstract

Met1 type ubiquitination and deubiquitination are involved in the regulation of many fundamental processes such as inflammation and innate immunity, and their interference by pathogens can suppress immune responses in human cells. However, no plant-derived deubiquitinases (DUBs) against Met1 ubiquitin chains have been reported. Using a dehydroalanine (DHA)-bearing Met1 diubiquitin (Met1-diUb) suicide probe, synthesized in one-pot, we identified OTUB1 from *Oryza sativa* (OsOTUB1) and uncovered its preference for Met1 ubiquitin chains. Also, by resolving the apo structure of OsOTUB1 and its complex with Ub or Met1-diUb, we demonstrated that OsOTUB1 hydrolyses Met1 ubiquitin chains by activation of both the distal and proximal ubiquitin, which is different from OTULIN and expands our mechanistic understanding of the DUB-mediated hydrolysis of Met1 ubiquitin chains. Through large-scale sequence alignment and hydrolysis experiments, two sites in the S1' pocket of the OTUB subfamily (OTUBs) were found to determine the hydrolytic ability of OTUBs against Met1 ubiquitin chains, regardless of species. Furthermore, by analyzing the species distribution of OTUBs capable of hydrolyzing Met1 ubiquitin chains, we found that whereas this activity does not exist in metazoans, it is conserved in green plants (*Viridiplantae*). This discovery may inform studies of the differentiation between primitive plants and animals.

Introduction

Ubiquitin can be attached to either one of the seven lysine residues (Lys6, Lys11, Lys27, Lys29, Lys33, Lys48, and Lys63) or N-terminal methionine (Met1) of another ubiquitin, allowing the formation of distinct ubiquitin chain configurations (Komander et al., 2012); and different types of ubiquitin chains add functional diversity to their linking proteins (Oh et al., 2018). Unlike ubiquitin chains linked with isopeptide bonds, linear ubiquitin chains (also known as Met1-linked chains, referred to hereafter as the “Met1 chains”) are connected by peptide bonds, the construction of which is catalyzed by linear ubiquitin chain assembly complex (LUBAC) in mammalian cells (Gerlach et al., 2011; Ikeda et al., 2011; Kirisako et al., 2006; Tokunaga et al., 2011). Met1 chains promote the activation of NF-κB signaling and autophagy by recruiting related downstream factors (Ikeda et al., 2011; Tokunaga et al., 2009). Deubiquitinases (DUBs) catalyze the hydrolysis of Met1 chains to negatively regulate the ubiquitination process, often modulating cell signaling. OTULIN (OTU deubiquitinase with linear linkage specificity) and CYLD (CYLD Lysine 63 deubiquitinase) are the only two types of DUBs that have been reported to hydrolyze the Met1 chains in mammalian cells (Hrdinka et al., 2017). More recently, RavD from a pathogenic microorganism (*Legionella pneumophila*) was also found to specifically depolymerize Met1 chains to weaken the host immune response (Wan et al., 2019).

The S1 and S1’ sites in DUBs are responsible for their specificity for the poly-Ub linkage: the S1 site guides the C terminus of the distal ubiquitin to the active center, while the S1’ site determines linkage selectivity by accommodating the distinct proximal Ub moiety. In some cases, the inactive configurations of S1 and/or S1’ rearrange and become active upon the binding of Ub substrate. OTULIN engages in one directional substrate-assisted catalysis wherein the proximal Ub of Met1-diub triggers the catalytic triad

rearrangement for activation. In contrast, the catalytic center and the overall structure of RavD does not undergo visible conformational changes upon binding to linear diUb, leading to the conclusion that the full activity of RavD is not predicated on substrate assistance (Wan et al., 2019).

In this manuscript, we report the identification of OsOTUB1, a homolog of human OTUB1 (hOTUB1) capable of the preferential hydrolysis of Met1 chains, by the screening of DUBs that can hydrolyze Met1 chains in *Oryza Sativa* using a dehydroalanine (DHA)-bearing Met1-diUb probe. OsOTUB1 is the first DUB known to deubiquitylate Met1 chains to be identified in a plant. Structural evidence demonstrated that OsOTUB1 hydrolyzes Met1 chains via a bi-modal activation mechanism wherein the distal Ub induces rearrangement and hence activation of the catalytic triad; and binding of the proximal Ub moiety triggers full activity of OsOTUB1 and the hydrolysis of Met1 chains. Three residues from two motifs located in the S1' pocket, henceforth referred to as the “M1-specific motif”, were identified as molecular determinants of the Met1 linkage specificity of OsOTUB1/hOTUB1. Furthermore, consensus sequence and conservation analysis of large-scale sequence alignments verified the prevalence of the M1-specific motif in nature. The conservation of these motifs in plants but not animals has implications for the study of their evolution.

Results And Discussion

1. **The discovery of plant DUBs that hydrolyze Met1 chains using an efficiently prepared Met1-diUb suicide probe**

To search for plant-based DUBs capable of cleaving Met1 chains, we designed and prepared a Met1-diUb active probe and used it to retrieve DUBs from northern japonica rice Zhonghua 11 (ZH11). Weber *et al*. reported an activity-based Met1-diUb probe containing DHA used for *in vitro* and *in vivo* functional analysis of OTULIN (Weber et al., 2017), but the synthetic approach used (total chemical synthesis) relied on multiple time-consuming procedures including chemical synthesis, HPLC purification, freeze drying, refolding etc. We developed a one-pot strategy capable of delivering about 100 mg of the probe within 10 hours (Fig. 1A). First, we recombinantly expressed and purified Met1-diUb bearing the N-terminus Avi-tag (GLNDIFEAQKIEWHE) (Lau et al., 2013) and incorporating a Gly76Cys mutation at the distal ubiquitin (**M1-diUb-1**). Then, the pH value of a solution of purified **M1-diUb-1** was adjusted to 9.5 using a mixture of 50 mM Tris•HCl and 150 mM NaCl. Subsequently, the biotin ligase BirA and 2,5-dibromohexanediamide, an alkaline elimination reagent, were incubated with **M1-diUb-1** at 37 °C. BirA specifically added biotin to Lys of Avi-tag (Lau et al., 2013), while 2, 5-dibromohexanediamide desulfurized the Cys76 of **M1-diUb-1** into DHA (Chalker et al., 2011). After nearly 8 hours, **M1-diUb-1** was almost 100% transformed into the biotinylated Met1-diUb probe bearing DHA (**M1-diUb-2**) (Fig. S1A, Supplementary_Experimental). To verify the efficacy of **M1-diUb-2**, we tested its crosslinking activity with OTULIN on a time gradient (Fig. S1C). The results showed that **M1-diUb-2** crosslinked with nearly 90% of OTULIN in 20 minutes, indicating that **M1-diUb-2** has an efficient crosslinking ability. Then, the crosslinked product (**M1-diUb-2**~OTULIN) was purified and used to assess its binding ability with streptavidin beads (Fig. S1D). The results showed that

streptavidin beads enriched **M1-diUb-2**~OTULIN efficiently after 30 min incubation. In summary, **M1-diUb-2** is well-suited to screen for plant DUBs with M1 activity.

To clarify whether DUBs with M1 activity exist in the plant kingdom, we used **M1-diUb-2** to retrieve DUBs from northern japonica rice Zhonghua 11 (ZH11) in the seedling stage (14 days). Rice seedlings were milled in liquid nitrogen and their proteins dissolved in lysis buffer. After centrifugation, **M1-diUb-2** was incubated with the supernatant at 37 °C to facilitate a crosslinking reaction. After enrichment by streptavidin beads and extensive washing, the proteins on beads were denatured in protein loading dye by heating and then separated by SDS-PAGE. Finally, each band on the gel was cut and degraded by trypsin. The digested peptides were separated by HPLC and analyzed by Orbitrap-MS/MS. Finally, the MS/MS spectra were searched against the rice.fasta downloaded from UniProt. The search criteria used were a fixed modification of carbamidomethyl (C); a variable modification of oxidation (M); precursor ion mass tolerances of 20 ppm, and a fragment ion mass tolerance of 0.02 Da. The peptide false discovery rate (FDR) was calculated using Percolator provided by Proteome Discoverer (PD). Peptide spectrum matches (PSM) were assumed correct for q values lower than 1%. FDR was determined based on PSMs when searched against the reverse decoy database. Peptides only assigned to a given protein group were considered as unique. In two independent experiments, five ubiquitin-related proteins were identified in the range of Score≥10, including 3 DUBs, OsUCH14, OsOTUB1, OsUCH-L, OsE1 and OsPolyUb (Fig. 1C). Coincidentally, these ubiquitin-related proteins are related to those found in human cells by Weber (Weber et al., 2017). For example, human-derived USP5, UCHL3, E1 and PolyUb identified by Weber correspond to OsUCH14, OsUCH-L, OsE1 and OsPolyUb, respectively (Weber et al., 2017).

To confirm the M1 activity of OsOTUB1 *in vivo*, we compared the differences in the abundance of Met1 chains between OsOTUB1 knockout and OsOTUB1 overexpressed transgenic seedlings. An antibody against Met1 chains was used to analyze the abundance of Met1 chains in the seedlings by western blot, and an antibody against Ub to check whether the total amount of Ub was affected (Fig. 1D). However, in the western blots, the intensities of the bands corresponding to Ub in wild-type, depleted, and overexpressed OsOTUB1 seedlings were almost the same, indicating that OsOTUB1 does not affect the total Ub in rice. Using the Met1 chains antibody, the intensity of the band corresponding to Met1 chains was slightly increased in OsOTUB1 knockout seedlings and significantly decreased in OsOTUB1 overexpressed seedlings, indicating that OsOUTB1 has M1 activity *in vivo* and therefore regulates the abundance of Met1 chains.

To further confirm the M1 activity of OsOTUB1 *in vitro*, we recombinantly expressed full-length OsOTUB1 (FL-OsOTUB1) and assessed its hydrolytic activity against eight types of diUb (Fig. 1E). FL-OsOTUB1 was found to effectively hydrolyze Lys48 diUb (<90%) but not Lys63 diUb (<10%) under the same conditions. This is consistent with a previous finding of Wang *et al.*, who proved that FL-OsOTUB1 preferentially cleaves Lys48 tetraUb (Wang et al., 2017). Unexpectedly, under the same conditions, FL-OsOTUB1 almost completely hydrolyzed Met1-diUb. In order to further confirm the preference of FL-OsOTUB1 for Met1 type,

we compared the activity differences of FL-OsOTUB1 against Met1- and Lys48-diUb (Fig. 1F). Under the same conditions, and at a FL-OsOTUB1: Met1/Lys48-diUb ratio of 1:30, FL-OsOTUB1 hydrolyzed 50% of Met1-diUb at 4 min, but only about 20% of Lys48-diUb, further demonstrating that FL-OsOTUB1 preferentially hydrolyzes Met1 chains. Notably, FL-OsOTUB1 was not stable (spots corresponding to it appeared diffuse on the gel, Fig. 1F) – perhaps due to degradation of the flexible, glycine-rich region on full-length protein (Fig. S2). Accordingly, we deleted the 73 residues at the N-terminus to obtain a truncated version of OsOTUB1 comprising only the sequence ranging from residues 74 to 324, but still incorporating the catalytic domain (OsOTUB1-cat). Biochemical experiments (Fig. 1F) showed that OsOTUB1-cat appeared on the gel as a single band, indicating it to be more stable. Fortunately, the preference of OsOTUB1-cat for Met1 chains was conserved as the full-length protein (hydrolyzes close to 80% of Met1-diUb at 4 min, while less than 50% for Lys48-diUb). Therefore, OsOTUB1-cat was used in all subsequent work, unless otherwise stated.

2. **Two-orientation activation mode of OsOTUB1-cat to Met1 chains**

To better understand the mechanism underlying the OsOTUB1-cat mediated degradation of Met1 chains, crystal structures of apo OsOTUB1-cat complexed with Met1-diUb or Ub were sought. OsOTUB1-cat crystals were grown in a reservoir containing 0.15 M potassium bromide and 30% w/v polyethylene glycol monomethyl ether 2,000. Using the catalytic domain structure of hOTUB1 (hOTUB1-cat) (PDB code 2ZFY) as the template, the crystal structure of OsOTUB1-cat at a resolution of 2.27 Å resolution (PDB code 6K9N, Fig. 2A, Supplementary_Table_1) was finally obtained after molecular replacement and refinement. The overall structure of OsOTUB1-cat was found to comprise 11 α-helices (α) and 5 β-sheets (β) and bear an active region at the interface between the α3 helix and the β5 sheet separating the S1 and S1’ pockets – almost identical to hOTUB1-cat (RMSD=1.46 Å) (Fig. 2B). Catalytic Cys121 is located at the end of the C-terminus of α3 helix (Fig. 2A). The imidazole ring of the catalytic His317 adopts a nearly vertical conformation with Cys121, and ε^2N is 6.8 Å away from the sulfur atom of C121 – much further than the distance between the catalytic His and Cys in the common DUBs (3~5 Å) (Kong et al., 2015; Mevissen et al., 2013), and too far for ε^2N to deprotonate the catalytic Cys. In summary, the catalytic triad configuration in OsOTUB1 is almost identical to that of hOTUB1-cat (Fig. 2B), and therefore the structural basis for their contrasting activities remains unknown.

To better understand how OsOTUB1-cat is activated and accomplishes the hydrolysis of Met1 chains, we attempted to resolve the crystal structure of OsOTUB1-cat crosslinked with Met1-diUb bearing DHA but not Avi (**M1-diUb-DHA**) (OsOTUB1-cat~**M1-diUb-DHA**). **M1-diUb-DHA** was first prepared in a manner analogous to that used for the one-pot preparation of **M1-diUb-2**, then incubated with OsOTUB1-cat at 37 °C, to allow the crosslinking reaction to proceed. Diffraction-quality crystals were finally obtained by crystallization from 0.2 M sodium chloride, 0.1 M BIS-TRIS pH 5.5, 25% w/v Polyethylene glycol 3350. The structures of apo OsOTUB1-cat and Ub (PDB code 1UBQ) were used as templates. After molecular

replacement and refinement, the complex crystal structure at a resolution of 2.34 Å (PDB code 6KBE, Fig. 2C, Supplementary_Table_1) was obtained.

The structures of OsOTUB1-cat~**M1-diUb-DHA** and apo OsOTUB1-cat (Fig. 2D) were compared, in an attempt to infer the mechanism for the activation of OsOTUB1-cat. We found that the γ amide of Gln2 in the proximal Ub ($Q2^{prox}$) is parallel to the imidazole ring of the catalytic His317 in the complex. Also, the orientation of the imidazole ring changes from being perpendicular to the catalytic Cys121 to being parallel to it, reducing the distance between the sulphur atom of catalytic Cys121 and the imidazole ring of catalytic His 317 from 6.8Å to 3.8Å, low enough for the imidazole ring to deprotonate the thiol (Fig. 2D). To uncover the role of $Q2^{prox}$, we mutated it to Ala ($Q2A^{prox}$) and examined the ability of OsOTUB1-cat to hydrolyze $Q2A^{prox}$ (Fig. 3E). After 8 min, OsOTUB1-cat had hydrolyzed only negligible amounts of Met1-diUb $Q2A^{prox}$; after 90 min, the conversion was still very low –only about 30%. However, under the same conditions, OsOTUB1-cat had hydrolyzed 50% of Met1-diUb after 8 minutes, indicating that the Q2A mutation in the proximal Ub significantly reduces the hydrolytic activity of OsOTUB1-cat. When $Q2^{prox}$ was mutated to Asn ($Q2N^{prox}$), OsOTUB1-cat had hydrolyzed about 30% of $Q2N^{prox}$ at 8 minutes, a slightly lower conversion compared with Met1-diUb, but an improvement compared to $Q2A^{prox}$. When $Gln2^{prox}$ was mutated to His ($Q2H^{prox}$), OsOTUB1-cat had hydrolyzed about 50% of Met1-diUb $Q2H^{prox}$ at 8 minutes, a similar rate of hydrolysis to that observed for the hydrolysis of Met1-diUb by OsOTUB1-cat, indicating that mutation of Q2H can restore the activity of OsOTUB1-cat. These results are ascribed to the contrasting accessibilities of the effective area: for Ala, the side chain cannot reach the effective area, making it unable to effectively activate OsOTUB1-cat; for Asn, the side chain is longer than that of Ala, but shorter than Gln, such that it can only partially reach the effective area, thus partially activating OsOTUB1-cat; for His, the side chain is large enough to reach the full effect area, effectively activating OsOTUB1-cat to a similar degree as that seen for Gln. In summary, the steric bulk of the side chains of three different residues influences the activity of OsOTUB1-cat (Fig. 3F). For the Glu mutation ($Q2E^{prox}$), although the side chain of Glu can reach the effective area, the negative charge of the pendant carboxyl group forms an electrostatic interaction with the positively charged imidazole ring of the catalytic His, preventing relocation of the imidazole ring to the active site, further diminishing the activity of OsOTUB1-cat (Only about 10% of $Q2E^{prox}$ was hydrolyzed at 90 minutes, significantly lower than in $Q2A^{prox}$). Summarizing the above results, we found that the side chain of $Gln2^{prox}$ can push the imidazole ring of catalytic His317 from a non-activated position to an activated position and further restrict the mobility of the imidazole ring at the activated position. In a previous study of the mechanism of the hydrolysis of Met1-diUb by OTULIN, we found that the imidazole ring of catalytic His339 can be liberated by $Glu16^{prox}$, which breaks the hydrogen bond formed between the imidazole ring of His339 and the inhibitory residue Asp336; and restricted by the sidechain of Gln2 at the activated position. This mechanism was previously characterized as a proximal Ub activation mechanism (Keusekotten et al., 2013). Here, we demonstrated that $Gln2^{prox}$ plays a similar role in the context of OsOTUB1-cat, and so we believe that there is also a proximal Ub activation mechanism at work in OsOTUB1-cat. It should be noted that the proximal Ub activation mechanism of OsOTUB1 is obviously different from that of OTULIN in that activation of

OsOTUB1 does not rely on the additional residue of proximal Ub to break the hydrogen bond imposed upon its catalytic imidazole; this is achieved only by the physical push from $Gln2^{prox}$.

These results demonstrated that the proximal Ub could activate OsOTUB1-cat, but the role played by the distal Ub in the activation process was still unclear. Accordingly, we investigated whether OsOTUB1-cat could hydrolyze Ub-7-amino-4-methylcoumarin (Ub-AMC) to ascertain whether DUB can be activated by the distal Ub by measuring the fluorescence of the free coumarin generated in the deubiquitination process (Fig. S3A). The results showed that under the action of OsOTUB1-cat, the fluorescence intensity of AMC continued to increase significantly, demonstrating that OsOTUB1-cat effectively hydrolyzes Ub-AMC (Fig. S3B). We then examined the ability of OsOTUB1-cat to crosslink with C-terminally propargylated Ub (Ub-PA) (Fig. 2G). The results showed that OsOTUB1-cat crosslinked >90% Ub-PA in 1 minute, consistent with the results of the Ub-AMC hydrolysis experiment. However, under the same conditions, OTULIN, which also has M1 activity, behaved differently: the fluorescence intensity generated by Ub-AMC hydrolysis was approximately equal to the background level (Fig. S3B), and only negligible concentrations of crosslinked products were detected, even after 30 min. The contrasting activities of OsOTUB1-cat and OTULIN against monoUb suggest that the activation of OsOTUB1-cat may be different from that of OTULIN. Previous studies have reported that OTULIN activation relies solely on the proximal Ub, preventing it from hydrolyzing Ub-AMC or crosslinking with Ub-PA (Keusekotten et al., 2013). Therefore, we believe that OsOTUB1-cat is activated by way of a distal Ub mechanism. To verify this, we resolved the crystal structure of OsOTUB1-cat crosslinked with Ub-PA (OsOTUB1-cat~Ub-PA). OsOTUB1-cat~Ub-PA was obtained by incubation OsOTUB1-cat with Ub-PA (see experimental) at 37 °C. After purification, conventional crystallization conditions were screened, and crystals meeting the diffraction requirements were finally obtained using 0.2 M sodium chloride, 0.1 M HEPES pH 7.5, and 25% w/v polyethylene glycol 3350. Using structures of apo OsOTUB1-cat and Ub as templates, the complex structure was finally resolved at a resolution of 2.34 Å after molecular replacement and refinement (PDB code 6K9P, Fig. 2H, Supplementary_Table_1). Based on this structure, binding of the distal Ub was found to induce a deflection of approximately 80 degrees and a distance reduction from 6.8 Å to 4.1 Å between side chains of the catalytic Cys121 and His317, forming an activated conformation. Therefore, the results proved that the distal Ub activates OsOTUB1-cat by inducing major conformational changes.

In summary, the hydrolysis of Met1 chains by OsOTUB1-cat relies on the activation of both proximal and distal Ub. This is in contrast to the activation of OTULIN that relies solely on activation of the proximal Ub. Our study has therefore revealed a novel mechanism for the DUB-mediated hydrolysis of Met1 chains.

3. **Two motifs in S1’ pocket determines Met1 type preference of OsOTUB1**

To determine the underlying mechanism for the preference of OsOTUB1 for Met1-type chains and understand the contrasting M1 activities of OsOTUB1-cat and hOTUB1-cat, we closely inspected the binding of Met1-diUb by OsOTUB1-cat. In OsOTUB1-cat~M1-diUb-DHA, the distal and proximal Ub moieties occupy the S1 and S1' pockets, respectively. The S1 pocket incorporates the hydrophobic patch of OsOTUB1-cat and consists of F225, F226, F229, L233, V256, I258, I259, L269, V271, Y273 and Y313. It

interacts with the hydrophobic patch of distal Ub, consisting of L8, I44, V70, L71 and L73. N267, D275, and H289 of OsOTUB1-cat interact with Q40 of the distal Ub via hydrogen bonds (Fig. S4A, B). Residues in OsOTUB1 responsible for the binding of distal Ub are conserved in hOTUB1 (Fig. S4C). Due to the high degree of structural similarity between hOTUB1-cat and OsOTUB1-cat, it seemed unlikely that the binding of the distal Ub to the S1 pocket could account for their significant differences in M1 activity.

Binding of the proximal Ub, E90, R314 and D319 of OsOTUB1-cat in the S1’ pocket to the E16 and K33 of Ub occurs via hydrogen bonds. In addition, residues of OsOTUB1 involved in the binding of proximal Ub are also conserved in hOTUB1 (Fig. S4C). However, based on the comparison of the primary sequences of hOTUB1 and OsOTUB1, the structure alignment between apo hOTUB1-cat and OsOTUB1-cat~M1-diUb-DHA showed two main variations: 1) the P87 of hOTUB1-cat at the entrance of catalytic center is different from G117 in OsOTUB1-cat; and 2) the G63, D64 and D65 residues of hOTUB1-cat (EDD), located in loop between α2 and α3, are different from S93, G94 and S95 in OsOTUB1-cat (SGS). In order to examine the effect of these two motifs on the M1 activity of OsOTUB1-cat, we first mutated the two motifs separately and simultaneously to the corresponding residues in hOTUB1-cat to obtain the separate mutants OsOTUB1-cat-G117P, OsOTUB1-cat-EDD, and the double mutant OsOTUB1-cat-G117P-EDD, and investigated their hydrolytic activities against Met1-diUb. The results showed (Fig. 3D) that mutation of any motif resulted in the detection of only negligible quantities of hydrolysis product, demonstrating both motifs to be essential for the M1 activity of OsOTUB1-cat. To further examine the role of these two motifs, we mutated the two motifs of hOTUB1-cat separately and simultaneously to the corresponding residues in OsOTUB1-cat to obtain the individual mutants hOTUB1-cat-P87G hOTUB1-cat-SGS and the double mutant hOTUB1-cat-P87G-SGS, and examined their hydrolytic activities against Met1-diUb. The results showed (Fig. 3D) that neither of the two single mutants could catalyze the formation of hydrolysis product, like wild type hOTUB1-cat. However, under the action of hOTUB1-cat-P87G-SGS, bands corresponding to hydrolysates appeared on SDS-PAGE, the intensities of which increased with time, indicating that mutations to both motifs are capable of conferring the M1 activity of hOTUB1-cat. In summary, these results establish that the residues of the two motifs in the S1’ pocket determine whether OsOTUB1-cat and hOTUB1-cat have M1 activity. Based on their order in the primary sequence, we named the SGS/EDD motif the N-handle motif, and the G/P motif the C-handle motif.

To understand the mechanism by which these two motifs affect M1 activity, we structurally analyzed their role in the interaction between the S1' pocket and the proximal Ub. 1) Analysis of C-handle motif. A key characteristic of Met1 chains is the repulsion between the bulky side chain of the Q2 residue of the proximal Ub and interacting proteins (Keusekotten et al., 2013). A similar repulsion cannot occur in OsOTUB1-cat since the G117 at the entrance of the catalytic center does not bear a side chain and cannot hinder the entry of the proximal Ub. However, because hOTUB1 bears the bulky and rigid P87 side chain, the proximal Ub is inaccessible, and therefore it does not exhibit M1 activity (Fig. 3A). 2) Analysis of N-handle motif. The SGS of OsOTUB1-cat does not bear any charge in a neutral environment, while EDD of hOTUB1-cat carries negative charges in a neutral environment. Analysis of the sequence of proximal Ub

revealed that D32, K33 and E34 in proximal Ub (DKE) is adjacent to the SGS/EDD region. Given the side chain of K33 is stabilized inside the Ub, DKE would also bear a negative charges in a neutral environment, and therefore would be electrostatically repulsed by the EDD motif of hOTUB1-cat, resulting in the inactivity of hOTUB1-cat against Met1 chains.

To furtherly clarify how the N-handle motif affects the binding of OsOTUB1-cat/ hOTUB1-cat to proximal Ub, and the extent to which this binding is dependent on electrostatic effects, we analyzed the interaction of the N-handle motif (S93, G94, S95) in OsOTUB1-cat with proximal Ub (Fig. 3F). We found that 1) the distances between the hydroxyl group of the side chain in S93 and the carboxyl groups of the side chain in E34 are 5.49 Å and 6.57 Å, respectively. Such distances are much larger than the distance usually associated with hydrogen bonds (≤4.0 Å), and therefore in OsOTUB1-cat the introduction of even an acidic amino acid with a long side chain, such as Glutamate (S93E), would still have no effect on M1 activity; 2) the closest distance between the hydroxyl group of the side chain in S95 and the carboxyl group of the side chain in D32 is 4.40 Å, a distance expected to be conducive to the formation of a hydrogen bond. Thus, the introduction of acidic amino acid with a short side chain, such as aspartic acid (S95D), would have a significant effect on M1 activity; 3) the α C of G94 is facing the loop structure of proximal Ub, 3.47 Å and 3.54 Å from the carbonyl oxygen in the backbone of Q31 and the nitrogen in the backbone of G35, respectively. This sterically crowded environment seems to exclude the entry of any side chain groups, such as methyl. To verify the above conjectures, we separately introduced S93E, G94A and S95D into the N-handle motif of OsOTUB1-cat and examined the hydrolysis activity of these mutants against Met1-diUb. The results showed (Fig. 3G) that OsOTUB1-cat-S93E hydrolyzed almost 50% of Met1-diUb at 4 minutes, comparable to that of OsOTUB1-cat (nearly 60% of Met1-diUb at 4 minutes) and indicating that the impact of S93E mutation is negligible. OsOTUB1-cat-S95D hydrolyzed almost 50% of Met1-diUb only after 30 min, indicating the effect of the S95D mutation to be significant. OsOTUB1-cat-G94A hydrolyzed less than 20% of Met1-diUb even after 30 min, and is therefore much less active than OsOTUB1-cat, demonstrating the major influence of the G94A mutation on catalytic activity. Based on these results, we concluded that in the N-handle motif, the van der Waals-free nature of side chain in G94 and the electrically neutral nature of side chain in S95 are conducive to the development of M1 activity, whereas S93 has a much smaller effect. Therefore, we can conclude the M1 activity-competent sequence in the N-handle motif is XGY, where X denotes any residue, and Y denotes any non-acidic residue.

To compare the effects of the N-handle and C-handle motifs on the M1 activity of OsOTUB1-cat, we assessed the activity of OsOTUB1-cat-G117P, OsOTUB1-cat-EDD, and OsOTUB1-cat-G117P-EDD against Met1-tetraUb in the presence of increased concentrations of enzyme and for prolonged hydrolysis periods (Fig. 3E). When the concentration of DUB was increased to 20 μM (DUB: Met1-tetraUb=2:1), approximately 100% of Met1-tetraUb disappeared after 60 minutes. However, Met1-tetraUb was little hydrolyzed by OsOTUB1-cat-G117P and not at all by OsOTUB1-cat-G117P-EDD. These results demonstrate that the C-handle motif more significantly influences the M1 activity of OsOTUB1-cat than the N-handle motif.

4. **The influence of the N-handle and C-handle motifs on M1 activity is observed in the OTUB subfamily from other species**

The above results established that the M1 activity of OsOTUB1-cat and hOTUB1-cat is determined by the characteristics of the residues of the N-handle and C-handle motifs of their S1’ pockets. To examine the generality of this observation, DUBs in the OTUB subfamily from other species were analyzed. Sequences of the C65 peptidase family (from the database Pfam), consisting of 1847 sequences from 874 species (PF10275, update to January 2020, Supplementary_PF10275_raw_data), which contains OTUB subfamily, were retrieved and sequentially analyzed by MEGA-X (Fig. 4A). First, sequences without catalytic activity were excluded based on analysis of the catalytic triad, leaving in 57% of the sequences to be analyzed in the next step. Second, these active sequences were studied to see which incorporated the C-handle motif (G-only) due to the necessity of this motif for M1 activity confirmed above; this was found in 68% of the active sequences. Third, these G-only sequences were studied to see which incorporated precisely three residues in the N-handle motif (G-only-ordered), because sequences of this pattern can be analyzed by our current model; this was found in 41% of the active sequences. Fourth, the G-only-ordered sequences were classified into five groups based on the residue composition in the N-handle motif: SGS, X'GS, XGN, XAD, and V, occupying 6%, 6%, 2%, 24%, and 3% of the active sequences, respectively, where X' represents any residue other than S, X represents any residue, and V (various) represents an irregular sequence pattern. Finally, the X’GS and XAD sequences were sub-classified into NGS, K/R-GS, G/A-GS, V1-GS, K/R-AD, N/Q-AD, S/T-AD and V2-AD based on the similarity of chemical properties of side chains. In these sequences, V1 (various 1) represents residue other than N, K, R, G and A, and V2 (various 2) represents residue other than K, R, N, Q, S and T. A total of 11 sequence patterns were obtained.

Statistical analysis of the G-only-ordered sequences showed that those incorporating irregular patterns (V, V1 and V2) comprised only a small proportion (13.02%). To simplify the analysis, we excluded all sequences with irregular patterns. Those with specific patterns, such as SGS, NGS, K/R-GS, G/A-GS, XGN, K/R-AD, N/Q-AD and S/T-AD, occupied 86.98% and 35.66% of G-only-ordered sequences and the active sequences, respectively. MEGA-X was used to calculate evolutionary distances between sequences under every pattern and OsOTUB1-cat, thus identifying the most evolutionally remote sequences. Given that most of the sequences analyzed originated from fungi, additional species were selected to broaden the range of species as much as possible. In total, fourteen candidate sequences were identified for recombinant expression and assessment of their hydrolysis activity against Met-diUb: AMAMU (*Amanita muscaria Koide* BX008), ZOSMR (*Zostera marina* (*Eelgrass*)) and AMBTC (*Amborella trichopoda*) in SGS mode; 9AGAR (*Hypholoma sublateritium* FD-334 SS-4) in NGS mode; 9TREE (*Kwoniella pini* CBS 10737) and RHOT1 (*Rhodosporidium toruloides* (strain NP11) *(Yeast)*) in K/R-GS mode; 9APHY (*Daedalea quercina* L-15889) and PHYPA (*Physcomitrella patens subsp. patens (Moss)*) in G/A-GS mode; WALI9 (*Wallemia ichthyophaga* (strain EXF-994/CBS 113033)) and GONPE (*Gonium pectorale (Green alga)*) in XGN mode; OPHP1 (*Ophiostoma piceae* (strain UAMH 11346) *(Sap stain fungus*)) in N/Q-AD mode; 9PEZI

(*Pseudogymnoascus sp.* VKM F-4519 (FW-2642)) and TRIHA (*Trichoderma harzianum (Hypocrea lixii)*) in K/R-AD mode; SPOSC (*Sporothrix schenckii* 1099-18) in S/T-AD mode. The results showed (Fig. 4B) that, under the almost same enzymatic concentration, sequences incorporating the patterns SGS, NGS, K/R-GS, G/A-GS and XGN hydrolyzed Met1-diUb, of which OTUBs from ZOSMR, 9APHY and GONPE had the highest activity, cleaving 40~50% Met1-diUb at 15 min. Those from AMBTC, 9AGAR, RHOT1, PHYPA and WALI9 had moderate activity, digesting 20~30% Met1-diUb at 15 min, and those from AMAMU and 9TREE had weak activity, hydrolyzing about 10% Met1-diUb at 15 min. All sequences incorporate the XGY pattern, confirming the association between XGY and M1 activity. In contrast, sequences incorporating the XAD pattern, including K/R-AD, N/Q-AD and S/T-AD, hydrolyzed negligible Met1-diUb within 15 minutes. Thus, in general, Met1-diUb hydrolytic activity is predicated on an N-handle motif of the XGY pattern, and a C-handle motif of G. Finally, these associations are conserved across species.

Of the peptidases in the C65 family, 341 are from fungi, 255 are from metazoan, and 76 are from green plants (*Viridiplantae*) (PF10275, update to January 2020, Supplementary_PF10275_raw_data); and 149 sequences incorporate the XGY-G pattern. In order to analyze the evolution pathway of the XGY-G pattern, we analyzed the distribution of species in which these 149 sequences were found (Supplementary_Alignment). The results showed that these 149 sequences comprised six obsolete sequences and 143 valid sequences, originating from 130 species including 66 species of green plants, ranging from unicellular plants, such as green algae (GONPE, *Gonium pectorale*), to multicellular plants, such as Indian rice (*Oryza sativa subsp. indica*), domestic barley (*Hordeum vulgare subsp. vulgare*), soybeans (*Glycine max*) and cocoa (*Theobroma cacao*) etc., together comprising 86.84% (66/76) of the total green plants in the C65 peptidase family. Thus, OTUBs from most green plants incorporate the XGY-G pattern, which means that OTUBs with M1 activity are conserved in almost all green plants – from lower plants to higher plants. However, in contrast, sequences incorporating the XGY-G pattern were not found in any metazoan. Therefore, we speculate that these differences in the sequences of the OTUBs in plants and animals and hence their contrasting propensities to hydrolyze Met1 chains already existed when the evolutionary paths of plants and animals diverged. Additionally, we note that sequences that conform to the XGY-G pattern are also present in 64 species of fungi, of which only 18.77% overlap with fungi species in the C65 peptidase family, indicating that OTUBs with M1 activity are likely not conserved in fungi. However, sequences derived from most plant-parasitic fungi do incorporate the XGY-G pattern, such as brown rot fungus (*Gloeophyllum trabeum (strain ATCC 11539/FP-39264/Madison 617)*), *Tilletia walker*, white rot fungus (*Ceriporiopsis subvermispora, strain B*), dwarf bunt fungus (*Tilletia controversa*), etc., implying that genes encoding for OTUBs with M1 activity in fungi might have transferred from plants during their co-evolution with plants, for example during their resistance against or adaption to plant immunity system (Fiil et al., 2013; Fiil et al., 2014; Hrdinka et al., 2017; Wan et al., 2019). Based on the above analysis, we speculated that OTUBs with M1 activity are unique in plants.

Discussion

Met1 chains has been intensively studied in animals and microorganisms but not plants – perhaps due to the lack of high-throughput probes. In this paper, we describe a one-pot method for preparing a Met1-

diUb probe carrying DHA, and then the application of this probe to screen DUBs in rice. Our synthetic method is based on the recombinant expression of Met1-diUb, and yielded about 100 mg of crystallization-competent probe in about 8 hours under conventional conditions, enough to support the acquisition of relatively large quantities of crosslinked protein complex samples for structural analysis by both x-ray and Cryo-EM techniques. Using probes prepared by this method, OTUB1 that preferentially hydrolyses Met1 chains and other proteins were discovered in rice. These proteins suggest the existence of regulators that preferentially recognize Met1 chains in plants. In recent studies, knockout or downregulation of OsOUTUB1 stabilized transcription factor OsSPL14 by enhancing its Lys63 poly-ubiquitination, and resulted in improved plant architectural characteristics such as a reduced tiller number, an increased grain number per panicle, and increased grain weight and yield (Wang et al., 2017). We demonstrated that knockout or overexpression of OsOTUB1 could increase or reduce the abundance of Met1 chains in rice, and speculated that manipulation of the gene encoding for OsOTUB1 might also affect the traits of rice by interfering the dynamics of Met1 chains in addition to affecting the modification of Lys63 poly-ubiquitination.

OTUBs that preferentially hydrolyze Met1 chains are widely distributed in plants. It has been reported that hOTUB1 specifically hydrolyzes Lys48 chains (Edelmann et al., 2009), and hOTUB2 hydrolyzes both Lys48 and Lys63 chains (Altun et al., 2015), but neither can hydrolyze Met1 chains. Here, we uncovered the differences in sequences of the M1 specific motif that account for these contrasting activities. Variation in the C-handle motif of the S1’ pocket has been previously reported to inhibit the hydrolysis of Lys63 chains by hOTUB1 but not hOTUB2 (Edelmann et al., 2009). Both the N-handle and C-handle motifs determine M1 chain selection. The XGY mode in the N-handle motif is widely distributed in *Viridiplantae* but not in *metazoan*, suggesting that it is plant-specific. Additionally, the XGY pattern is also widespread in plant parasitic fungi, suggesting that DUBs with M1 activity and incorporating the XGY pattern may be involved in the modulation of plant immunity, similar to the function of RavD from the animal parasite *Legionella pneumophila* (Wan et al., 2019). In the OTU family, the C-handle motif participates in the selectivity of the Lys63 chains in addition to participating in the selectivity of the Met1 chains. Therefore, compared to the C-handle motif, the N-handle motif is widely distributed in plants with a specific feature of M1 selectivity.

The finding that OsOTUB1 has M1 activity extends the linkage selectivity range of DUBs in the OTUB subfamily, from Lys48 and Lys63 to Met1. In addition, results from our large-scale sequence alignment study showed that two motifs competent for Met1 selectivity are ubiquitous in the OTUB subfamily DUBs of plants, ranging from lower unicellular plants to higher multicellular plants, but not in animals. Recent studies have sequenced and analyzed the genome and transcriptome of *Mesostigma viride*, a unicellular plant positioned at the base of the Streptophyta clade, and deepened our understanding of the evolution of land plants from unicellular aquatic ancestors (Liang et al., 2020). We do not yet know when primitive unicellular organisms began their evolution into plants or animals, and how to distinguish the primitive unicellular organisms which traveled along different evolutionary paths. Here, taxonomically, the molecular features determining members of OTUB subfamily can hydrolyze Met1 chains could constitute

a molecular marker to distinguish between plants (where these features are conserved) from animals (where they are not).

Previously studies established that OTU family enzymes are activated either by the proximal Ub or distal Ub. As a member of the OTU family, OTUB1 can crosslink with Ub-PA, suggesting that it is activated by distal Ub (Mevissen et al., 2013). We validated a previous study showing that apo hOTUB1 adopts an inactivated state characterized by mismatch of the catalytic triad. However, the successful crosslinking of hOTUB1 with Ub-PA proved its activation by distal Ub. In contrast, OTULIN cannot crosslink with Ub-PA, but is nevertheless capable of hydrolyzing Met1-diUb, indicating that OTULIN activation is reliant on proximal Ub alone, an observation supported by structural biology (Keusekotten et al., 2013). Here, we report for the first time that OsOTUB1 relies on activation of both the distal and proximal Ub, wherein the distal Ub induces the realignment of the catalytic triad in a manner similar to most distal Ub mediated activation, and the Gln2 residue of the proximal Ub activates OsOTUB1 by pushing and locking the catalytic imidazole in His at the active site. It should be noted that the proximal Ub activation mode associated with OsOTUB1 is different from that of OTULIN. In apo OTULIN, an Asp positioned outside of the active site stabilizes the catalytic imidazole away from the active site by a hydrogen bond, which is broken by the Glu16 of the proximal Ub before the catalytic imidazole is pushed and locked at the active site by the Gln2 of the proximal Ub (Keusekotten et al., 2013). But this process does not occur in OsOTUB1, wherein the neutral amide group of the Gln2 residue in the proximal Ub pushes and locks the catalytic imidazole ring at the active site (the breaking of a hydrogen bond is not needed). This previously unknown activation process of OsOTUB1 suggests that members of the OTUB subfamily may have evolved functional differentiation in the course of the evolution of the species from which they are found.

Declarations

Conflict of interest

The authors declare no conflict of interest.

References

Altun, M., Walter, T.S., Kramer, H.B., Herr, P., Iphofer, A., Bostrom, J., David, Y., Komsany, A., Ternette, N., Navon, A.*, et al.* (2015). The human otubain2-ubiquitin structure provides insights into the cleavage specificity of poly-ubiquitin-linkages. PLoS One *10*, e0115344.

Chalker, J.M., Gunnoo, S.B., Boutureira, O., Gerstberger, S.C., Fernández-González, M., Bernardes, G.J.L., Griffin, L., Hailu, H., Schofield, C.J., and Davis, B.G. (2011). Methods for converting cysteine to dehydroalanine on peptides and proteins. Chemical Science *2*, 1666-1676.

Edelmann, M.J., Iphofer, A., Akutsu, M., Altun, M., di Gleria, K., Kramer, H.B., Fiebiger, E., Dhe-Paganon, S., and Kessler, B.M. (2009). Structural basis and specificity of human otubain 1-mediated deubiquitination.

Biochem J *418*, 379-390.

Fiil, B.K., Damgaard, R.B., Wagner, S.A., Keusekotten, K., Fritsch, M., Bekker-Jensen, S., Mailand, N., Choudhary, C., Komander, D., and Gyrd-Hansen, M. (2013). OTULIN restricts Met1-linked ubiquitination to control innate immune signaling. Mol Cell *50*, 818-830.

Fiil, B.K., and Gyrd-Hansen, M. (2014). Met1-linked ubiquitination in immune signalling. FEBS J *281*, 4337-4350.

Gerlach, B., Cordier, S.M., Schmukle, A.C., Emmerich, C.H., Rieser, E., Haas, T.L., Webb, A.I., Rickard, J.A., Anderton, H., Wong, W.W.*, et al.* (2011). Linear ubiquitination prevents inflammation and regulates immune signalling. Nature *471*, 591-596.

Hrdinka, M., and Gyrd-Hansen, M. (2017). The Met1-Linked Ubiquitin Machinery: Emerging Themes of (De)regulation. Mol Cell *68*, 265-280.

Ikeda, F., Deribe, Y.L., Skanland, S.S., Stieglitz, B., Grabbe, C., Franz-Wachtel, M., van Wijk, S.J., Goswami, P., Nagy, V., Terzic, J.*, et al.* (2011). SHARPIN forms a linear ubiquitin ligase complex regulating NF-kappaB activity and apoptosis. Nature *471*, 637-641.

Keusekotten, K., Elliott, P.R., Glockner, L., Fiil, B.K., Damgaard, R.B., Kulathu, Y., Wauer, T., Hospenthal, M.K., Gyrd-Hansen, M., Krappmann, D.*, et al.* (2013). OTULIN antagonizes LUBAC signaling by specifically hydrolyzing Met1-linked polyubiquitin. Cell *153*, 1312-1326.

Kirisako, T., Kamei, K., Murata, S., Kato, M., Fukumoto, H., Kanie, M., Sano, S., Tokunaga, F., Tanaka, K., and Iwai, K. (2006). A ubiquitin ligase complex assembles linear polyubiquitin chains. EMBO J *25*, 4877-4887.

Komander, D., and Rape, M. (2012). The ubiquitin code. Annu Rev Biochem *81*, 203-229.

Kong, L., Shaw, N., Yan, L., Lou, Z., and Rao, Z. (2015). Structural view and substrate specificity of papain-like protease from avian infectious bronchitis virus. J Biol Chem *290*, 7160-7168.

Lau, P.N., and Cheung, P. (2013). Elucidating combinatorial histone modifications and crosstalks by coupling histone-modifying enzyme with biotin ligase activity. Nucleic Acids Res *41*, e49.

Liang, Z., Geng, Y., Ji, C., Du, H., Wong, C.E., Zhang, Q., Zhang, Y., Zhang, P., Riaz, A., Chachar, S.*, et al.* (2020). Mesostigma viride Genome and Transcriptome Provide Insights into the Origin and Evolution of Streptophyta. Adv Sci (Weinh) *7*, 1901850.

Mevissen, T.E., Hospenthal, M.K., Geurink, P.P., Elliott, P.R., Akutsu, M., Arnaudo, N., Ekkebus, R., Kulathu, Y., Wauer, T., El Oualid, F.*, et al.* (2013). OTU deubiquitinases reveal mechanisms of linkage specificity and enable ubiquitin chain restriction analysis. Cell *154*, 169-184.

Oh, E., Akopian, D., and Rape, M. (2018). Principles of Ubiquitin-Dependent Signaling. Annu Rev Cell Dev Biol *34*, 137-162.

Tokunaga, F., Nakagawa, T., Nakahara, M., Saeki, Y., Taniguchi, M., Sakata, S., Tanaka, K., Nakano, H., and Iwai, K. (2011). SHARPIN is a component of the NF-kappaB-activating linear ubiquitin chain assembly complex. Nature *471*, 633-636.

Tokunaga, F., Sakata, S., Saeki, Y., Satomi, Y., Kirisako, T., Kamei, K., Nakagawa, T., Kato, M., Murata, S., Yamaoka, S.*, et al.* (2009). Involvement of linear polyubiquitylation of NEMO in NF-kappaB activation. Nat Cell Biol *11*, 123-132.

Wan, M., Wang, X., Huang, C., Xu, D., Wang, Z., Zhou, Y., and Zhu, Y. (2019). A bacterial effector deubiquitinase specifically hydrolyses linear ubiquitin chains to inhibit host inflammatory signalling. Nat Microbiol *4*, 1282-1293.

Wang, S., Wu, K., Qian, Q., Liu, Q., Li, Q., Pan, Y., Ye, Y., Liu, X., Wang, J., Zhang, J.*, et al.* (2017). Non-canonical regulation of SPL transcription factors by a human OTUB1-like deubiquitinase defines a new plant type rice associated with higher grain yield. Cell Res *27*, 1142-1156.

Weber, A., Elliott, P.R., Pinto-Fernandez, A., Bonham, S., Kessler, B.M., Komander, D., El Oualid, F., and Krappmann, D. (2017). A Linear Diubiquitin-Based Probe for Efficient and Selective Detection of the Deubiquitinating Enzyme OTULIN. Cell Chem Biol *24*, 1299-1313 e1297.

Figures

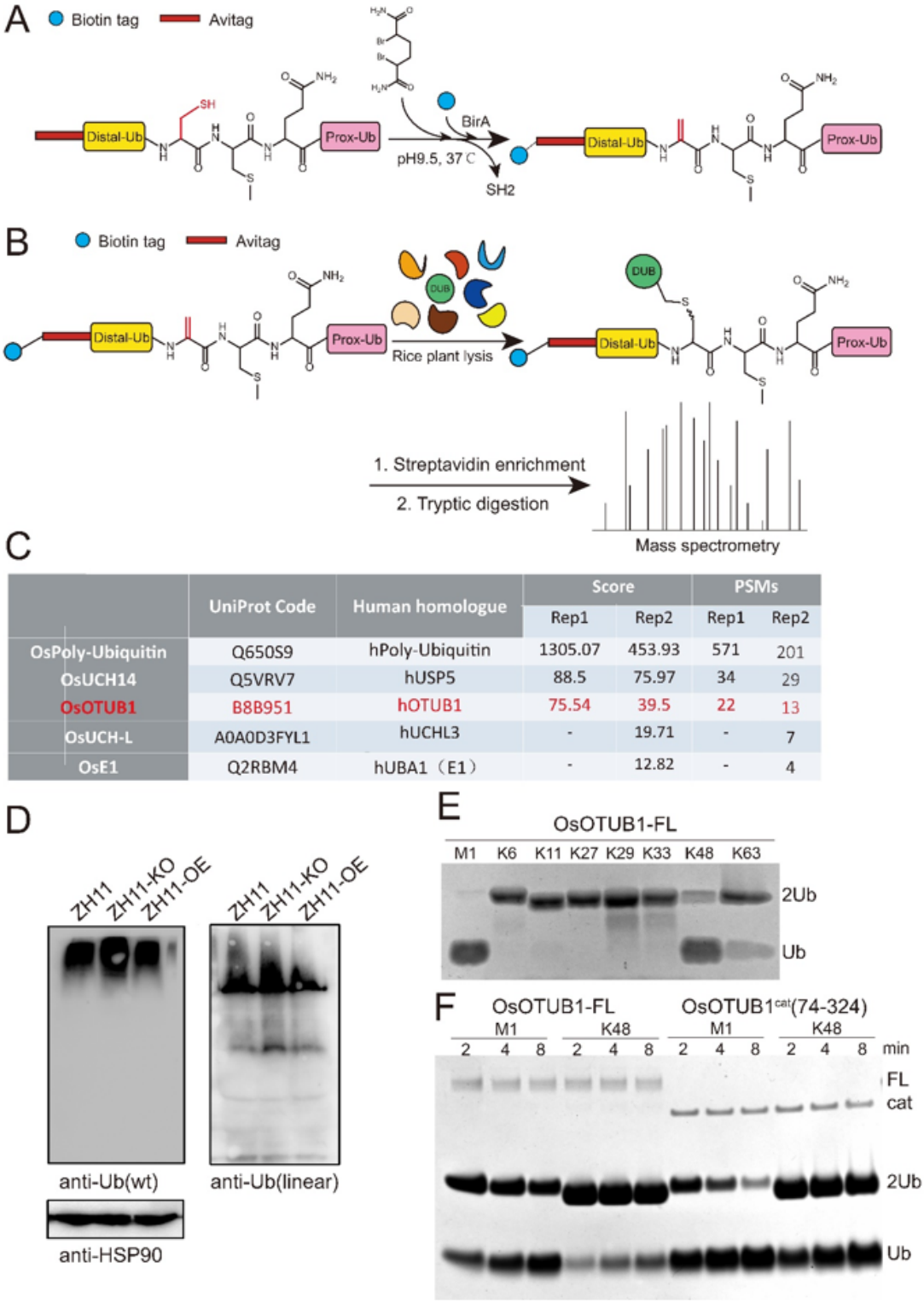

	UniProt Code	Human homologue	Score		PSMs	
			Rep1	Rep2	Rep1	Rep2
OsPoly-Ubiquitin	Q650S9	hPoly-Ubiquitin	1305.07	453.93	571	201
OsUCH14	Q5VRV7	hUSP5	88.5	75.97	34	29
OsOTUB1	B8B951	hOTUB1	75.54	39.5	22	13
OsUCH-L	A0A0D3FYL1	hUCHL3	-	19.71	-	7
OsE1	Q2RBM4	hUBA1（E1）	-	12.82	-	4

Figure 1

Use of the probe M1-diUb-2 to identify OTUB1 in Oryza sativa, and show that OTUB1 depolymerizes M1 chain in vivo and preferentially hydrolyzes M1 chain in vitro A, The one-pot synthesis of M1-diUb-2; B, The identification of DUBs that hydrolyze the M1 chain in Oryza Sativa using M1-diUb-2; C, Ubiquitin related hits by mass spectrometry; D, Effects of OsOTUB1 over-expression and knockout on the abundance of M1 chain; E, Hydrolysis activity against 8 linkage-type diUbs by recombinantly expressed full-length

OsOTUB1; F, Time-scale hydrolysis activity of OsOTUB1 (full-length and the catalytic domain) against M1- and K48-diUb. KO, knock out; OE, overexpression; FL, full-length; cat, catalytic.

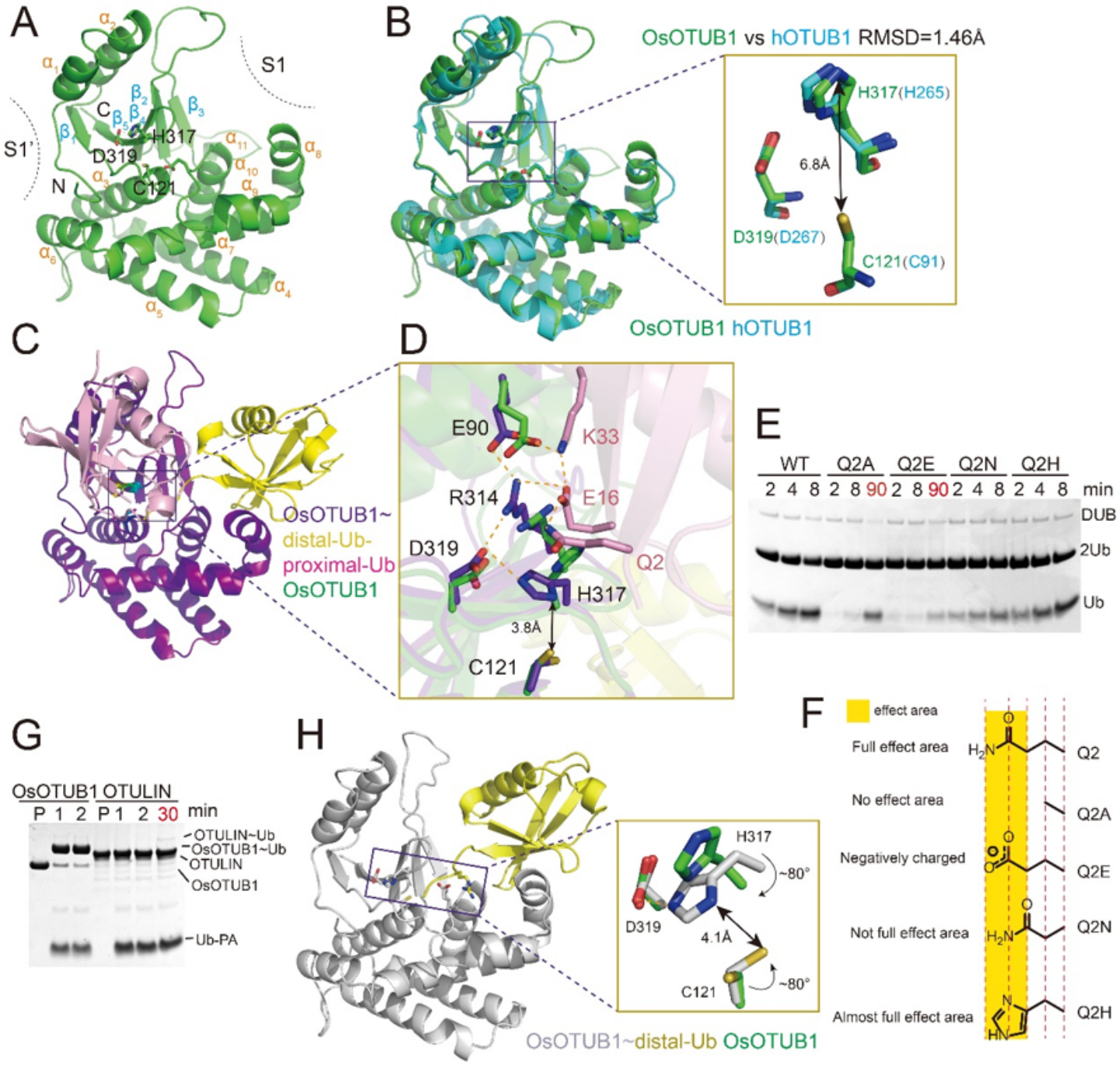

Figure 2

Dual directional activation A, Crystal structure of OsOTUB1-cat; B, Structural alignment between OsOTUB1-cat and hOTUB1-cat; C, Crystal structure of OsOTUB1-cat~M1-diUb-DHA; D, Structural alignment between catalytic centers of OsOTUB1-cat and OsOTUB1-cat~M1-diUb-DHA; E, Effects of Q2 mutation in the proximal Ub on M1-diUb hydrolytic activity; F, Mechanism for proximal Ub assisted

activation; G, Time scale Ub-PA crosslinking activity of OsOTUB1 and OTULIN; H, Crystal structure of OsOTUB1-cat~Ub-PA.

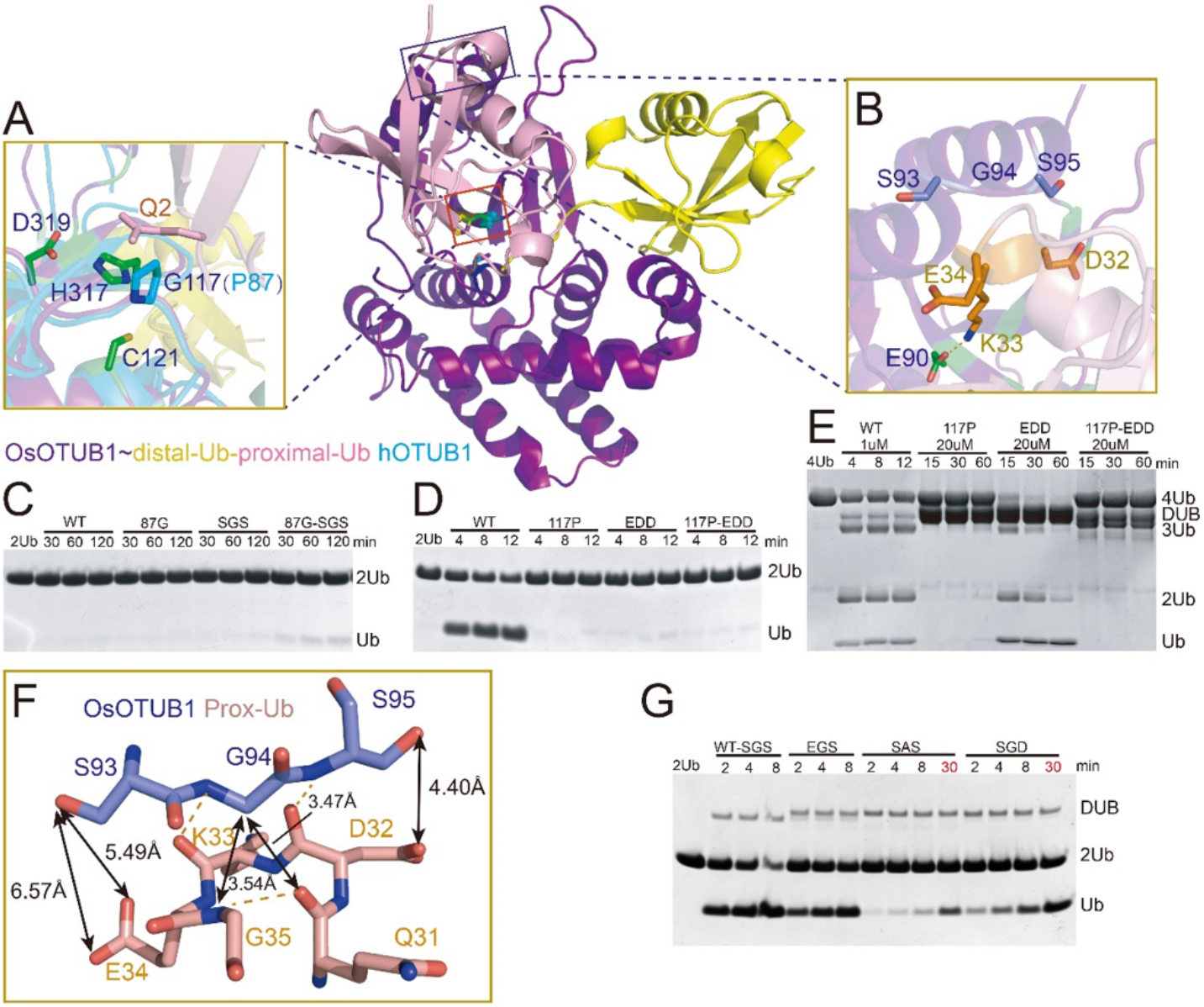

Figure 3

Two motifs in S1’ pocket determine M1 linkage selectivity of OsOTUB1 A, Structural alignment between C-handle motifs of OsOTUB1-cat~M1-diUb-DHA and hOTUB1-cat; B, Interface between OsOTUB1 and proximal Ub in OsOTUB1-cat~M1-diUb-DHA; C, Effects of mutations in two motifs on the hydrolysis activity of hOTUB1-cat against M1-diUb; D, Effects of mutations in two motifs on the hydrolysis activity of OsOTUB1-cat against M1-diUb; E, Effects of mutations in two motifs on the hydrolysis activity of OsOTUB1-cat against M1-tetra-Ub when the reaction concentration of OsOTUB1-cat was elevated to 20 μM; F, Detail interaction between N-handle motif of OsOTUB1 and proximal Ub; G, Effects of mutations in N-handle motif on the hydrolysis activity against M1-diUb.

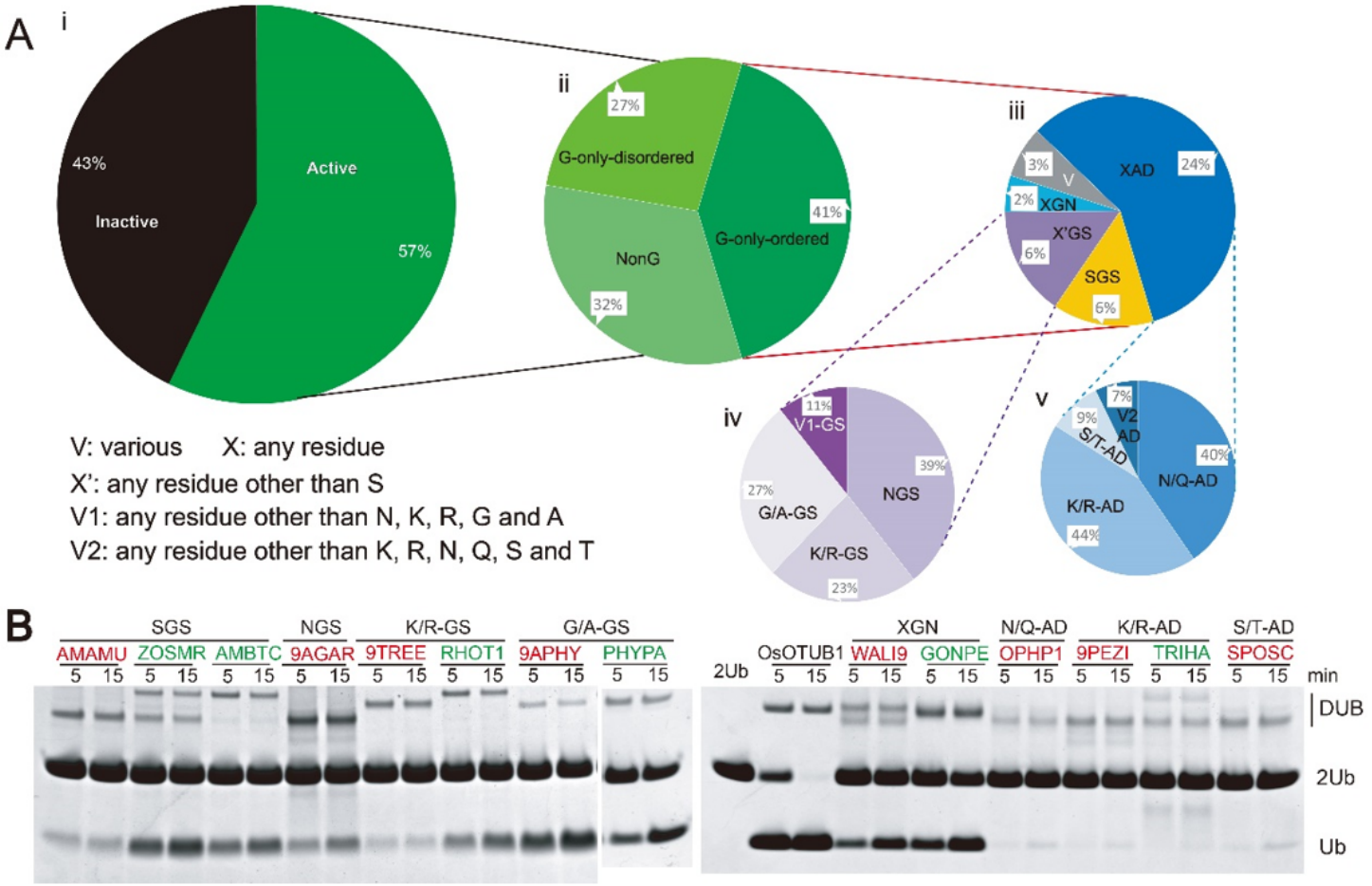

Figure 4

M1-specific motif rule is prevalent in members of OTUB subfamily A, Classification of C65 peptidase family based on characterization of catalytic triad and residues in two motifs of S1' pocket; B, Hydrolysis activity against M1-diUb by representative DUBs in every category. DUBs labeled with red are the evolutionarily remotest ones from OsOTUB1, while that labeled with green are species rather than fungus. AMAMU, Amanita muscaria Koide BX008; ZOSMR, Zostera marina; AMBTC, Amborella trichopoda; 9AGAR, Hypholoma sublateritium FD-334 SS-4; 9TREE, Kwoniella pini CBS 10737; RHOT1, Rhodosporidium toruloides NP11; 9APHY, Daedalea quercina L-15889; PHYPA, Physcomitrella patens subsp. patens; WALI9, Wallemia ichthyophaga, EXF-994/CBS 113033; GONPE, Gonium pectoral; OPHP1, Ophiostoma piceae, UAMH 11346; 9PEZI, Pseudogymnoascus VKM F-4519; TRIHA, Trichoderma harzianum; SPOSCS, Porothrix schenckii 1099-18.

Supplementary Files

This is a list of supplementary files associated with this preprint. Click to download.

- SupportingInformation.docx